Pergamon

CEMENT AND CONCRETE RESEARCH

Cement and Concrete Research 29 (1999) 133–142

Pore structure of cement silica fume systems Presence of hollow-shell pores[1]

Knut O. Kjellsen [a,*], Elisabeth Helsing Atlassi [b]

[a]*Swedish Cement and Concrete Research Institute, Stockholm, Sweden*
[b]*Department of Building Materials, Chalmers University of Technology, Gothenburg, Sweden*

Manuscript received 28 August 1998; accepted manuscript 14 September 1998

Abstract

Significant amounts of "hollow-shell" pores (i.e., Hadley grains) have been found in mature Portland cement-based systems containing silica fume. Hollow-shell pores were found directly by electron microscopy and were indicated by desorption isotherms. Hollow shells are an intrinsic type of pore, along with capillary pores and gel pores. They are large pores enclosed in cement gel and connected to the outside via gel and capillary pores. At low water-to-binder ratios they can be more than two orders of magnitude larger than the capillary pores, and they may constitute a porosity larger than that of capillary pores. Despite self-desiccation effects, hollow-shell pores seem to remain largely saturated with pore fluid. The smaller capillary pores dry before hollow-shell pores. The development of hollow-shell pores and their preservation at later ages in cement silica fume systems is discussed.

Keywords: Pore size distribution; Microstructure; Water vapor desorption isotherms; Silica fume; Sulfate-resistant cement; High-performance concrete

Different types of intrinsic pores exist in cement paste and concrete: gel pores and capillary pores. Recently, the presence of hollow-shell pores as a third type of intrinsic pore has been postulated on the basis of electron optical evidence [1]. As the cement grains recede due to hydration, stable hydrates may or may not form within the boundaries of the original cement particles. Hydrates formed within the peripheries of the original cement grains are termed "inner" products, whereas hydrates formed outside, in the capillary pore space [2], are termed "outer" products [3]. As it sometimes can be problematic to distinguish between "inner" and "outer" product using the electron microscope, various modifications of the concept of "inner" and "outer" product have been suggested [4–6].

When stable hydrates do not form within the original cement grain boundaries, a pore space is established, which represents a pseudoform of the dissolved cement phase. Such pores are often termed "hollow shells," "hollow-shell" pores, or "Hadley grains" [7]. It has been demonstrated that they are not the result of specimen preparation [8,9], and they have not been mixed with other types of pore [1,9]. Indeed, a mode of cement hydration leading to the formation of hollow shells is a very important mode in the hydration of cement, at least in the hydration of low-alkali sulfate-resistant cements [1]. By 1 day most of the hydrated cement had, in fact, left hollow shells [1]. At later ages, inner products are increasingly formed, implying that the presence of hollow shells diminishes. However, it seems that, in cement silica fume systems, hollow shells largely persist at later ages and may constitute a very significant porosity [1].

Hollow shells are large pores and are about the size of smaller cement grains. At low water-to-binder (w/b) ratios, they can be larger than the capillary pores by more than two orders of magnitude [1]. In mature systems, in particular, hollow-shell pores are embedded in cement gel containing much smaller gel and capillary pores. Because of their strong "ink-bottle" nature they may not easily be detected by many indirect methods for pore structure characterization, for example, mercury intrusion porosimetry (MIP). A number of MIP studies have revealed that when parts of the cement are replaced by silica fume, the "threshold pore diameter," as defined by Winslow and Diamond [10], and the volume of pores intruded by mercury decrease [11–15]. The results have been interpreted as "a refinement of the pore structure" brought about by the presence of silica fume. However, it is also possible that many large hollow-shell pores were present in the systems with silica fume, but were not detected due to the so-called "ink-bottle effect." The

* Corresponding author. Knut O. Kjellsen's present address, Norcem A.S., R&D Department, P.O. Box 38, N-3950 Brevik, Norway. Tel.: 47-3557-2000; Fax: 47-3557-0400; E-mail: Knut.kjellsen@norcem.scancem.com.

[1] This paper was originally submitted to *Advanced Cement Based Materials* on 21 August 1997 and accepted on 24 August 1998. The paper was received at the Editorial Office of *Cement and Concrete Research* on 28 August 1998 and accepted in final form on 14 September 1998.

0008-8846/99/$–see front matter
PII: S0008-8846(98)00166-5

presence of hollow shells may, in fact, be a major reason for the recorded reduction of the threshold pore diameter and the reduced intrusion of mercury. These topics are addressed in the present paper.

This paper reports experimental results on the influence of silica fume on the microstructure and pore structure of mature cementitious systems. The quantity and characteristics of hollow-shell pores, and their preservation at later ages particularly, are discussed. The results of numerous energy dispersive X-ray analyses will be reported at a later stage. The microstructural development at early ages is discussed elsewhere [1,8]. The pore structure was studied directly by scanning electron microscopy (SEM) on flat polished sections and indirectly by water vapor desorption isotherms. The paper is part of a larger project researching the hydration and microstructure of high-performance concrete.

1. Experimental

1.1. Materials, mixing, and curing

Paste and mortar specimens were made of Portland cement, condensed silica fume (csf), deionized water, and a superplasticizer. A quartz sand was used in the mortars. Paste specimens were made for SEM examination, whereas mortars were made for the desorption experiments. The cement used was a Swedish low-alkali sulfate-resistant cement (corresponding to ASTM type V). The characteristics of the cement and csf are as described by Kjellsen et al. [1]. The csf was in slurry form and contained 50% solids. The superplasticizer was composed of 40% sulfonated naphthalene formaldehyde, 0.3% tributyl phosphate, and water. The w/b ratios were 0.25 and 0.40. The binder contained either 0 or 10% csf by weight. The paste-to-sand ratio of the mortars was 1.0 by volume. The mass of superplasticizer was 3% or 4% in the 0.25 w/b ratio mixes without or with csf, respectively. At 0.40 w/b ratio, the mass of superplasticizer was 0.5% or 1.5% in the mixes without or with csf, respectively. Mixing was performed so as to assure that the csf was well dispersed [1].

The curing temperature was 20°C. To prevent segregation of the paste specimens, the molds were completely sealed and slowly rotated for at least 12 hours before they were opened. The paste specimens were placed in tightly sealed glass bottles containing only a very small amount of air. The mortars were cured in two ways; one set of specimens was sealed in thick rubber membranes while the other set was placed in confined plastic containers containing lime water. Curing in the sealed glass bottles or rubber membranes ensured that practically no moisture was lost or gained from the specimens. Carbonation was avoided.

1.2. Microscopy

SEM backscattered electron (BSE) images of 9-month-old paste specimens were obtained. The JEOL 6400 SEM was operated at 10 kV, and the working distance was 8 mm. SEM energy dispersive X-ray analysis was performed to identify various phases. Epoxy impregnated and flat polished specimens were examined. Samples were sawn out of the paste specimens. Hydration was stopped by freeze drying. The specimens were finally dried at 105°C overnight and were subsequently vacuum impregnated with a low-viscosity epoxy resin. They were then very carefully ground and polished down to 0.25 μm. Alcohol was used as lubricant during cutting and grinding, whereas diamond pastes were used as the polishing compound. The specimens were finally coated with carbon. Additional details of the specimen preparation procedure were provided previously [9]).

1.3. Desorption isotherms

After 3 months of curing in sealed containers, or in water, the cast mortar bars (40/40/160 mm) were cut into discs about 1.5 mm thick. The discs of the water-cured bars were stored in lime water for 1 week to obtain full saturation. The discs were placed in desiccators over saturated salt solutions of LiCl, $MgCl_2$, K_2CO_3, NaBr, NaCl, KCl, KNO_3, K_2SO_4, and distilled water, respectively. The temperature was 20°C. The water vapor pressures thus obtained provided relative humidities (RHs) of about 11%, 33%, 43%, 59%, 75%, 86%, 94%, 98%, and 100%, respectively. The specimens were subjected to the various environments for up to 3 months. Periodic registration of their weight indicated that constant weight was practically reached after 3 months. A precise weight equilibrium may never be reached because of structural changes that may occur on prolonged exposure under the various environments [16]. The RH was measured on dummy specimens and showed, at the time of the final weight registrations, RHs corresponding reasonably well to their surrounding environment. Measures were taken to avoid carbonation during the experiment. The evaporable water content, W_e/B, was determined on the basis of drying at 105°C. The denominator, B, refers to the mass of binder (i.e., cement plus csf). Preliminary tests showed that the paste and the mortar specimens provided practically identical desorption isotherms. It should be noted that the isotherms of the specimens cured under sealed conditions are not true desorption isotherms. Because of self-desiccation effects, the RH in the specimens at the start of the experiments will be considerably lower than 100%. The part of the isotherms above the RH in the seal-cured specimens is actually a scanning curve, meaning that the seal-cured specimens will absorb water rather than loose water in the upper range of water vapor pressures.

2. Results

2.1. Microscopy

2.1.1. Systems without silica fume

Fig. 1 provides a view of the 0.40 w/b ratio paste without silica fume (csf). The cement grains appear almost white,

CH appears light gray, other reaction products appear generally as darker gray, and pores appear black in BSE images. It can be observed that relatively few anhydrous cement grains remain unreacted after 9 months. An analysis showed the degree of cement hydration to be about 74%. However, most of the ferrite phase remains unreacted, as in all the examined specimens [17]. Ferrite is observed as the brightest anhydrous phase in the image.

Early in the hydration process, CH may form as large crystals in the capillary pore space [18]. These are often observed as massive regular crystals and sometimes as irregular formations in flat polished sections; their formation may be restricted by obstacles such as the boundaries of the tortuous capillary pore space. Examples of CH that are likely to be of this origin are marked with black circles in Fig. 1. CH also may form as slender platy crystals in the capillary pore space, mostly observed as elongated thin rods in flat polished sections. At later ages, CH particles with the size and regular shape of smaller cement grains also may be observed. Examples are indicated by black crosses in Fig. 1. Our experience is that CH particles of this form are not observed very often at early ages (e.g., Figs. 3–5 of [8]). A few large pores are observed; these are hollow shells that will be discussed. A couple of these are partially hollow shells with remnant belite phases; these are outlined by squares. The BSE image in Fig. 2 shows a close-up from the upper central part of Fig. 1. A partially hollow shell is outlined in Fig. 2. The striated structure and size and shape of feature indicate that it is a hydrated belite grain. X-ray analysis showed the upper part to consist of C-S-H, whereas the brighter, more porous lower part is essentially CH. Whereas alite leaves hollow shells at early ages [1,8], belite may, at later ages, hydrate according to a hollow-shell mode, with the formation of partially hollow shells with a characteristic

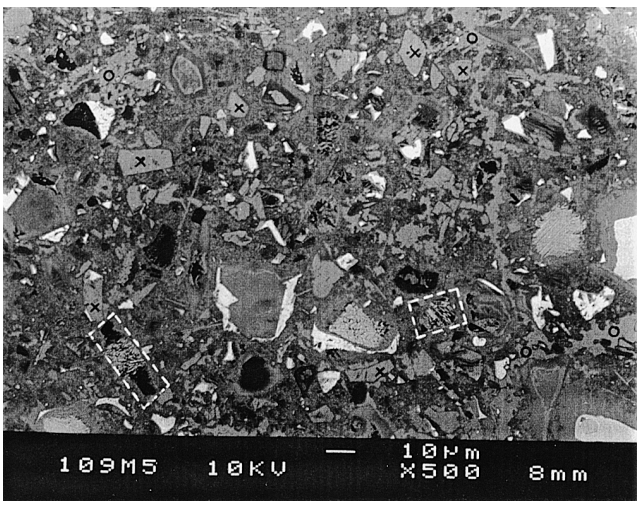

Fig. 1. BSE image of the 0.40 w/b ratio paste without silica fume. Small black circles indicate irregularly shaped CH phases; black crosses indicate CH particles with the distinct shape of cement grains; squares indicate partially hollow shells with remnant belite phases.

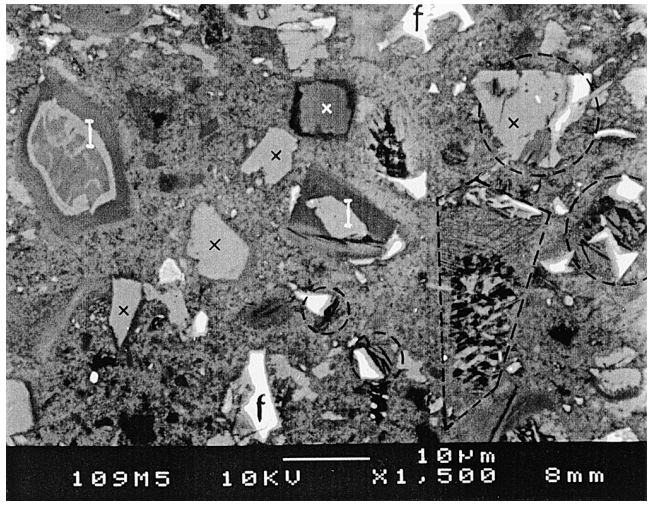

Fig. 2. Detailed BSE image from the upper central part of Fig. 1. f, ferrite; I, inner product phase of C-S-H/CH; black crosses indicate CH particles with the distinct shape of cement grains; circles indicate assemblages of CH/AFm/ferrite; white cross indicates a large AFm particle.

striated structure [1]. CH particles, with the size and shape of cement grains, are observed and marked with black crosses. The phenograins (i.e., distinct microstructural features) [6] "I" contain products of C-S-H (darker phases) and CH (brighter phases). CH and AFm phases often are observed in relation to remaining ferrite phases; examples are outlined by circles. The brightest areas of these features are anhydrous ferrite; CH phases are darker than ferrite phases, whereas AFm phases are darker than CH phases. AFm phases sometimes appear cracked. A large AFm particle is seen toward the top of the image and is marked with a white cross.

A view of the 0.25 w/b ratio paste without csf is depicted in Fig. 3. The degree of cement hydration is about 58% [17]. Relatively few hollow shells are observed; some of the par-

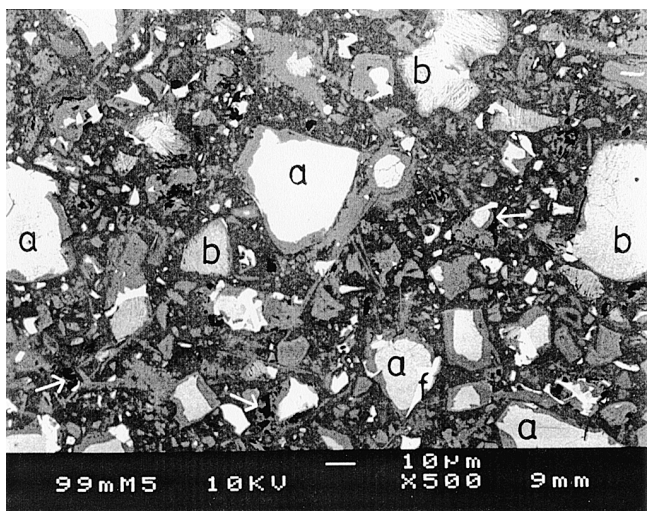

Fig. 3. BSE image of the 0.25 w/b ratio paste without silica fume. a, alite; b, belite; f, ferrite; arrows indicate partially hollow shells.

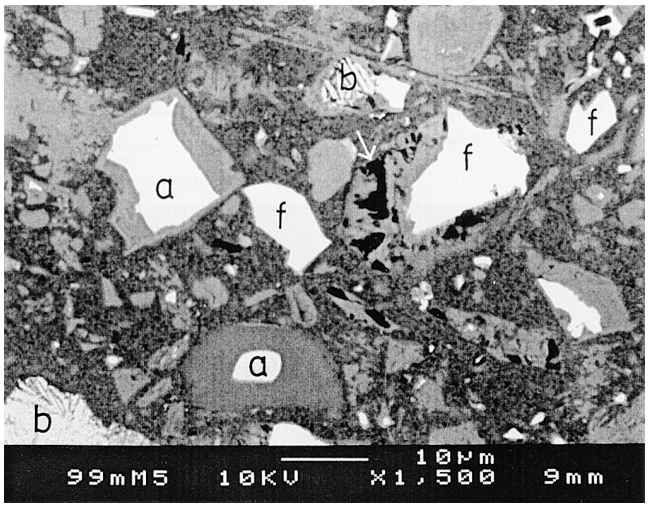

Fig. 4. Detailed BSE image from the lower part of Fig. 3. a, alite; b, belite; f, ferrite; arrow indicates partially hollow shell.

tially hollow shells are marked with arrows. Fig. 4 depicts a detailed area from the lower part of Fig. 3. Bright phases of what are considered to be essentially inner products are seen around most alite grains. These bright phases are mostly of C-S-H, sometimes also of CH, or mixtures of the two. Presumably because of the restricted capillary pore space of this low w/b ratio paste, the type of continuous and highly irregular CH phases frequently seen at the higher w/b ratio are observed to a much lesser extent now. However, the CH particles with the size and distinct shape of cement grains also are found extensively in this low w/b ratio paste. They are difficult to distinguish from the relatively dense C-S-H "inner" product phases. However, energy dispersive X-ray analysis showed that many of these features, with the size and shape of cement grains, were of CH.

2.1.2. Systems with silica fume

Fig. 5 depicts a BSE image of the 0.40 w/b ratio paste with csf. The degree of cement hydration is about 74%, all csf has reacted [17]. The microstructure appears more homogeneous than in the pastes without csf (Figs. 1–4). One reason for this is the pozzolanic reaction between csf and CH, which has resulted in conversion of csf and CH to C-S-H. Another characteristic feature of this paste with csf is the presence of many hollow-shell pores. Examples are denoted by arrows. Fig. 6 shows a detailed area from the central part of Fig. 5. Some of the hollow-shell pores are marked with arrows. When they are partially hollow at this stage, they often contain ferrite phases and some reaction products. In cement grains originally composed of alite and ferrite phases, the alite phase may hydrate completely, often leaving a partially hollow shell with remnant unreacted ferrite phases. The CH observed in the "outer" product often appears discontinous and intermixed with C-S-H. This is typical of mixes containing csf. One such area is outlined in Fig. 6. The phenograin "I" consists of a remnant ferrite phase (very bright triangular shaped phase), products of C-S-H (darker gray), and a surrounding rim of CH (bright rim). The many distinct CH particles, with the size and shape of cement grains, which were observed frequently in the pastes without silica fume, are much more seldom seen when csf is present. A partly hydrated belite grain is marked with a "b."

Fig. 7 shows a BSE image of the 0.25 w/b ratio paste with csf. The degree of cement hydration is about 50%. Practically all csf has reacted [17]. An apparent difference from the pastes without csf is the presence of considerably more hollow-shell pores. As with the 0.40 w/b ratio paste, the presence of distinct CH phases is much less pronounced when csf is present. Also, the bright distinct phases of essentially inner product commonly seen around remnant alite cores in the pastes without csf are not often observed when

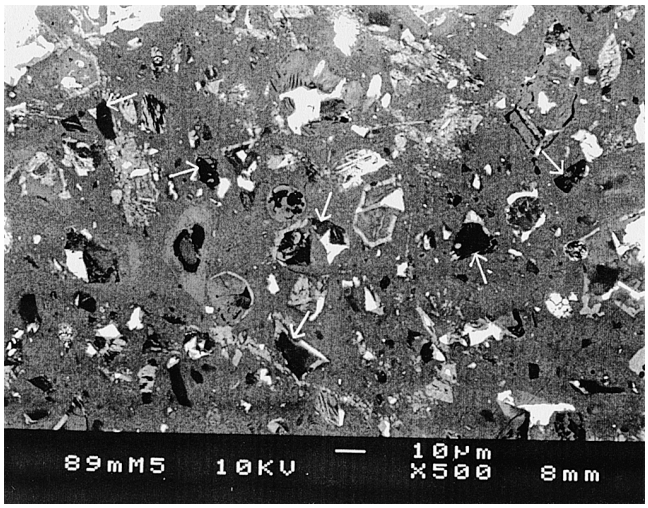

Fig. 5. BSE image of the 0.40 w/b ratio paste with silica fume. Arrows indicate hollow-shell pores.

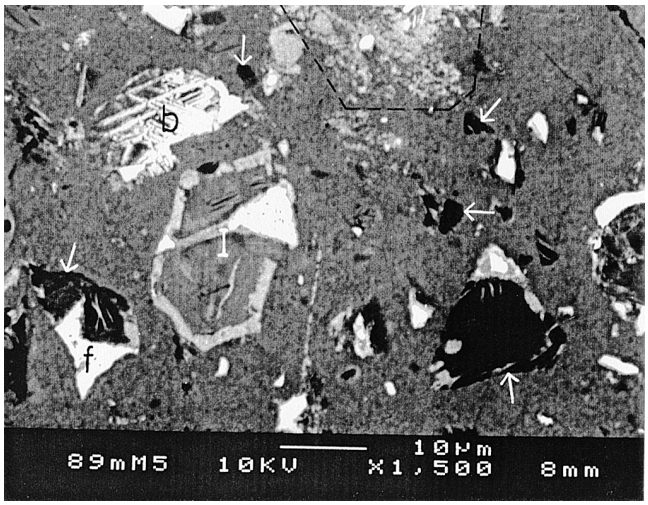

Fig. 6. Detailed BSE image from the central part of Fig. 5. b, belite; f, ferrite; I, inner product phase of C-S-H/CH; arrows indicate hollow shells; area of discontinous CH is outlined.

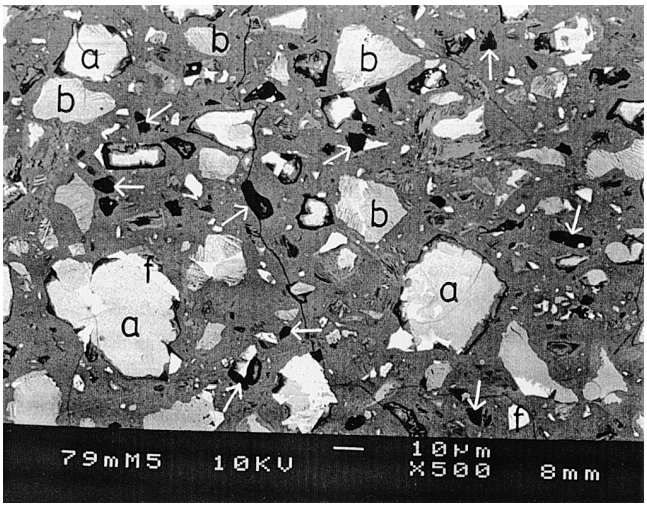

Fig. 7. BSE image of the 0.25 w/b ratio paste with silica fume. a, alite; b, belite; f, ferrite; arrows indicate hollow shells.

csf is present. There is often a separation between what is considered to be essentially inner and outer product. Fig. 8 shows an area from the central part of Fig. 7 in detail. Hollow shells are marked with arrows. Large phases of AFm are marked with white crosses.

2.2. Desorption isotherms

Figs. 9 and 10 depict the water vapor desorption isotherms of the 0.40 and 0.25 w/b ratio pastes, respectively. Sealed curing conditions imply that a certain internal desiccation (i.e., self-desiccation) occurs as the volume of chemical shrinkage is not refilled with water. The water-treated specimens, on the other hand, represent a state of practically full water saturation. The additional evaporable water present in the water-treated specimens corresponds quite

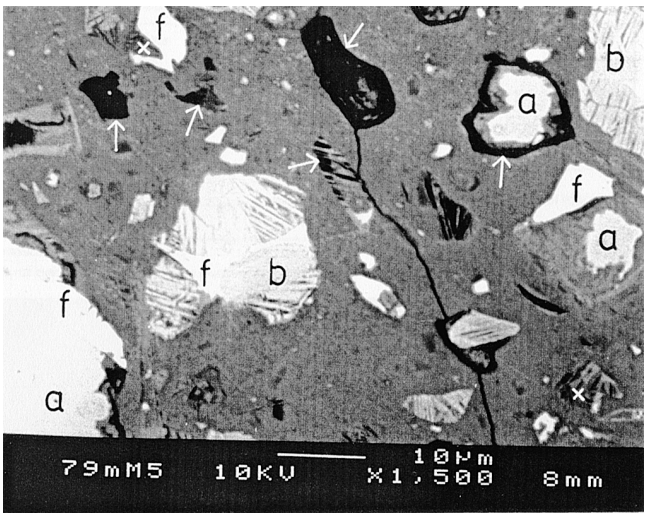

Fig. 8. Detailed BSE image from the central part of Fig. 7. a, alite; b, belite; f, ferrite; arrows indicate hollow shells; white crosses indicate AFm.

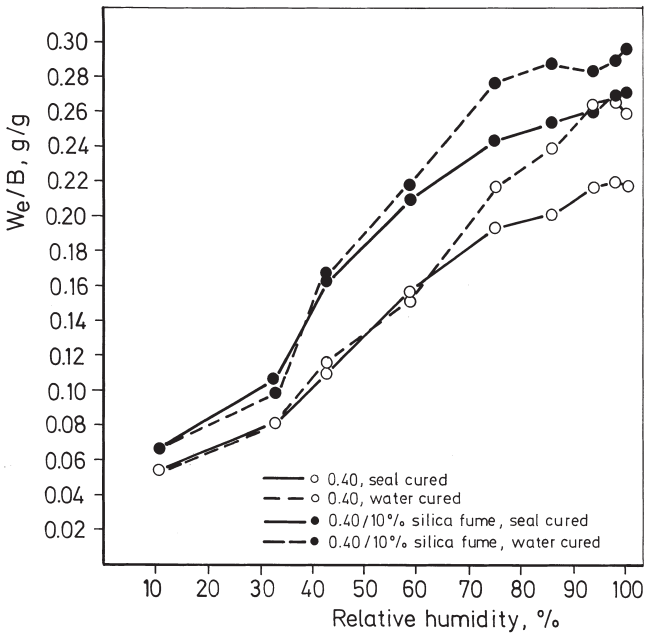

Fig. 9. Water vapor desorption isotherms of the water-cured and seal-cured 0.40 w/b ratio systems, with or without silica fume.

well to the calculated volume of chemical shrinkage. It seems that the 0.25 w/b ratio specimens have gained some extra hydration due to the water treatment. This is indicated by the slightly higher evaporable water content at 11% RH and a slightly higher nonevaporable water content.

Fig. 11 shows the difference in evaporable water content between the water-cured and the seal-cured specimens in the different RH intervals. It is observed from Figs. 9–11

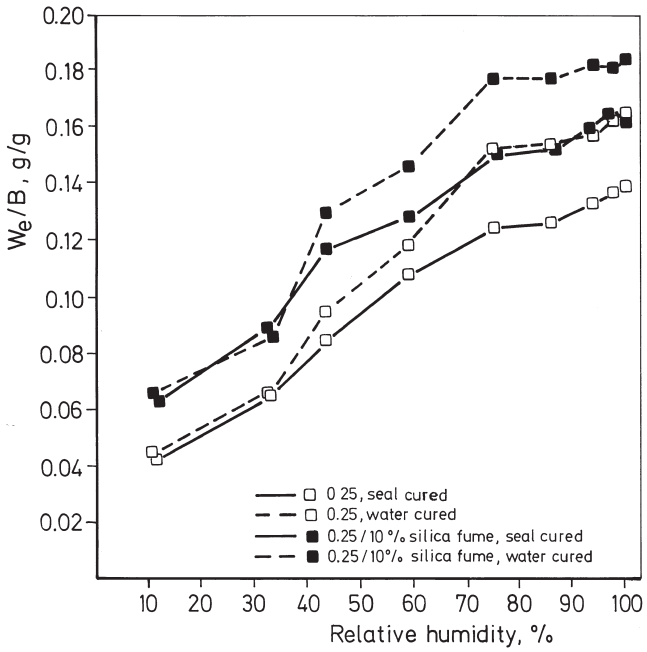

Fig. 10. Water vapor desorption isotherms of the water-cured and seal-cured 0.25 w/b ratio systems, with or without silica fume.

that most of the additional water present in the water-treated samples is evaporated at relatively high humidities. Practically all the additional water present in the water-treated 0.40 w/b ratio systems has evaporated at an RH of 59%. Most of the additional water present in the water-cured 0.25 w/b ratio systems is evaporated at RHs in the 75% to 43% range. Some additional water is evaporated between 43% and 33% RH. The results indicate that, upon self-desiccation, it is primarily the water present in the larger continous pores (i.e., capillary pores) that is desiccated. The negative values for three of the mixes in the 100% to 75% RH interval in Fig. 11 presumably occur because the isotherm of the seal-cured specimens in this upper region is a scanning curve and not a desorption curve (c.f. experimental section).

Fig. 12 shows the ratio between the evaporable water content of the systems with csf and the systems without csf, in the different RH intervals. The presence of csf increases the amount of evaporable water held at lower RHs, particularily in the 0–11% and 33–43% ranges, and decreases the amount of evaporable water held at higher RHs. This effect is seen in Figs. 9 and 10 as an increasing convex shape of the isotherms when the systems contain csf. This principal effect of csf on the desorption isotherm has been observed previously [11,16,19–21].

2.3. Evaluation of desorption isotherms: Relation to pore structure

Water vapor desorption isotherms provide information about the radius of pore (openings) through which the pore water may evacuate upon drying. The relationship between the approximate diameter of the opening to a pore that will be emptied at a certain RH is given by the Kelvin equation as follows: 11% RH—15Å; 33% RH—25Å; 43% RH—35Å; 59% RH—50Å; 75% RH—90Å; 86% RH—160Å; 94% RH—400Å 98% RH—1000Å.

The evaporable water content at 11% RH may be taken as a measure of the specific surface area of the specimen, or as a measure of the amount of C-S-H gel [22]. Based on the Kelvin equation, the desorption isotherms (Fig. 10) indicate that there are very few pores that are connected to the outside by pore openings larger than about 90Å at w/b ratio 0.25. At w/b ratio 0.40, the diameter of the largest “entryway” pore sizes decreases from about 400Å to about 160Å, when csf is incorporated (Fig. 9).

Apart from an apparent reduction in entryway pore sizes and an increased amount of evaporable water content retained at 11% RH, the presence of csf implies a notable increase in the amount of evaporable water desiccated in the 43% to 33% RH range, corresponding to pore openings between about 25 and 35Å. This can, in principle, be due to the presence of a considerable amount of gel pores, or extremely fine capillary pores, in this narrow range of pore sizes. Alternatively, the considerable loss of evaporable water of particularely the systems with silica fume upon desiccation between 43% and 33% RH is due to the presence of larger pores embedded in a gel matrix of much smaller pores. The small entryway pores leading to the larger pore would still be about 25 to 35Å in diameter. Helsing Atlassi [16,20,21] obtained both desorption and absorption isotherms from systems with and without csf. The desorption isotherms were, in principle, identical to those shown in Figs. 9 and 10. The specific loss of evaporable water between 43% and 33% RH from the system with csf was evident. The hysteresis effect between desorption and absorption was much stronger when csf was present. The absorption data indicated that, in the 33% to 43% RH interval, a porosity not greater than that corresponding to that of the gel isotherm was readsorbed. Thus, the specific porosity desiccated between 43% and 33% RH, present primarily in

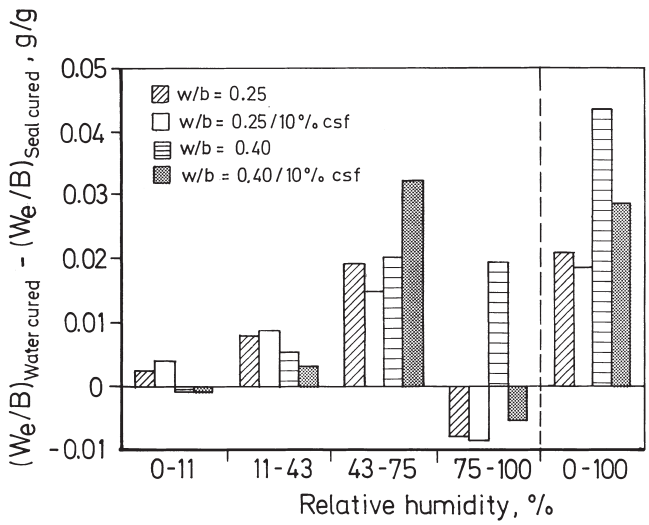

Fig. 11. Difference in evaporable water content (W_e/B) between the water-cured and seal-cured specimens, for different relative humidity intervals.

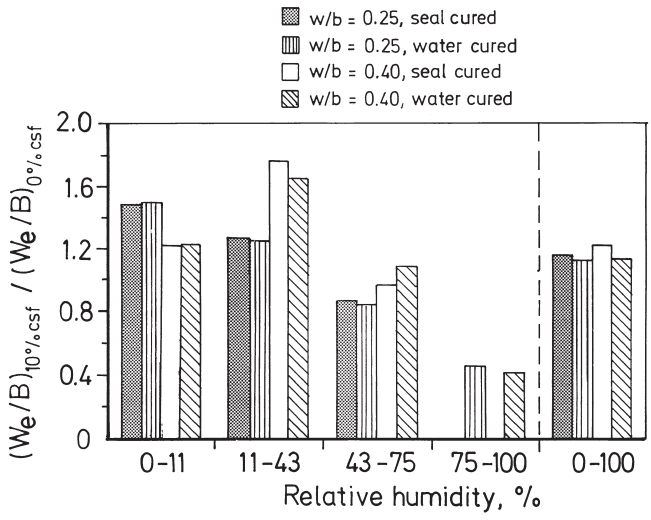

Fig. 12. Ratio between the evaporable water content (W_e/B) of the systems with silica fume and the systems without silica fume, respectively, for different relative humidity intervals.

the csf systems, was apparently reabsorbed at considerably higher RHs than those from which they were desiccated. More water was absorbed at very high RHs, above 94%, when csf was present. This type of strong hysteresis effect, obtained in the systems with csf in particular, is characteristic of the presence of "ink-bottle" pores. "Ink-bottle" pores will be drained at water vapor pressures corresponding to the size of their entryway pores, whereas they should be refilled at water vapor pressures corresponding to their own sizes. The observations provide a strong indication that the amount of evaporable water removed between 43% and 33% RH, corrected for the contribution from the gel isotherm, is removed from "ink-bottle" pores with largest entryway pores of the size of "coarse" gel pores. If this particular porosity dessicated at water vapor pressures corresponding to between 43 and 33% RH had been gel pores or extremely fine capillary pores, they should have been readsorbed at water vapor pressures similar to those at which they were desiccated, but were not. The "ink-bottle" pores indicated from the desorption isotherms in the 43% to 33% RH interval can be hollow-shell pores and/or possibly enclosed capillary pores, for example. The result from the section on microscopy and a previous paper [1] show direct evidence of hollow-shell pores.

Various types of porosities have been obtained on the basis of the water vapor desorption isotherms (Figs. 9 and 10). On the basis of calculations, the results are given in Table 1. The porosities were calculated according to Powers and Brownyard [22]. Three months' hydration data necessary for these calculations is as given in [17]. The measured total porosity is obtained from the total evaporable water content. The evaporable water content at 11% RH was used to establish "gel isotherms" and, thus, gel porosities in accordance with Powers and Brownyard [22]. The measured total porosity and the gel porosity increase with the presence of csf, which is in agreement with previous findings based on similar experiments [11,15,19,20]. The loss of evaporable water in the 43% to 33% RH range, corrected for the contribution from the gel isotherm, is taken as an "ink-bottle" porosity. The results from both seal-cured and water-cured specimens are given in Table 1. Kjellsen et al. [1] measured the hollow-shell porosity by image analysis. The results obtained after 3 months of hydration are given in Table 1. The measures of "ink-bottle" porosity obtained from the desorption isotherms are in good agreement with the hollow-shell porosity obtained by image analysis. Measures of capillary porosity were obtained by subtracting the gel porosity and the hollow-shell porosity from the total porosity. The measured total porosity and the obtained gel porosity agree reasonably well with the calculated values. It can be seen from Table 1 that at a w/b ratio of 0.40, the system with csf has a somewhat lower hollow-shell porosity than capillary porosity. However, in the 0.25 w/b ratio system with csf, the hollow-shell porosity is larger than the capillary porosity. The porosity constituted by hollow shells may represent around 20% of the total porosity when csf is present, and up to about 10% in the systems without csf.

As shown previously (Figs. 9–11), the desorption isotherms indicate that it is primarily the capillary pores that become drained upon self-desiccation. At w/b ratio of 0.40, the gel- and hollow-shell pores appear to remain saturated upon self-desiccation, as the desorption isotherms of the water- and seal-cured specimens are practically identical below 43% RH. At a w/b ratio of 0.25, the isotherms of the seal- and water-cured specimens do not join each other until an RH of 33%. It is very likely that parts of the water in the hollow-shell pores are drained upon self-desiccation in this case. The volume of chemical shrinkage is larger than the capillary porosity.

Table 1
Various types of porosity as obtained from desorption isotherms, microscopy, and theoretical calculations

	Water-to-binder ratio/silica fume (%)			
	0.40/0	0.40/10	0.25/0	0.25/10
Total porosity				
Desorption isotherms	37.1	40.7	30.7	32.4
Calculated	37.7	—	26.9	—
Gel porosity				
Desorption isotherms	18.3	21.8	17.5	25.4
Calculated	19.7	—	18.7	—
Ink bottle porosity				
Desorption isotherms				
Seal cured	3.1	7.9	2.7	3.2
Water cured	4.0	8.3	4.1	6.1
Hollow-shell porosity				
Microscopy	2.5	9.1	2.2	4.9
Capillary porosity				
Experimental	16.3	9.8	11.0	2.1
Calculated	18.0	—	8.3	—

3. Discussion

3.1. Formation and preservation of hollow shells

After a rim of hydration products forms on the cement grains early in the hydration process, the cement gel mostly grows outward, into the capillary pore space (i.e., as outer products). A void space (i.e., hollow shell) may develop within the boundary of the original cement grains as the cement grains recede on continued hydration. A mode of hydration leading to hollow shells appears to be the dominating hydration mode up to the age of 1 day [1]. Smaller grains of alite may hydrate completely, leaving completely hollow shells after about 1 day. Larger alite grains will not have hydrated completely at the same age, thus leaving hollow shells with remnant anhydrous cores [1,8].

Later in the hydration process, outer products continue to form while, simultaneously, inner products are increasingly formed. This implies that those partially hollow shells established relatively early in the hydration process, with hollow-shell separations dividing remnant anhydrous alite

cores and product (c.f. Figs. 4 and 5 of [8]), later may become filled with fresh hydration products, mainly C-S-H. The formation of inner product phases of essentially C-S-H at later ages is observed clearly in the systems without csf but not so extensively in the systems with csf (Figs. 1–8). CH may form in apparently complete hollow shells, whereas AFm often forms in hollow shells containing remnant ferrite phases. That AFm and CH phases form in previously established hollow shells is indicated by the fact that they often have the size and shape of cement grains. Although CH crystals also form at early ages, they seldom then have the size and shape of cement grains. AFm largely forms at somewhat later ages, when the capillary pores of the relatively low w/b ratio systems studied are much smaller than the size of the large AFm formations. The only pores corresponding to their size are hollow shells. This provides a clear indication that these phases have formed in hollow shells established earlier in the hydration process. AFm, in particular, is often observed in relation to remnant ferrite phases in distinct assemblages. Ferrite is a source of Fe, which probably does not readily migrate outside the boundary of the original cement grain due to its low solubility in an alkaline environment [23]. Thus, the Fe-containing AFm phases may preferably form in hollow shells containing remnant ferrite, where Fe is provided by the hydration of the ferrite and where the crystals have room to grow. The formation of CH and AFm at relatively late ages in previously formed hollow shells is similar to the formation of these phases in water-saturated cracks or air voids. Crystal growth preferably occurs in larger water-filled spaces [24]. The desorption isotherms do indicate that the hollow-shell pores to a large extent remain saturated with pore fluid under seal-curing conditions.

The formation of reaction products in previously established hollow shells, primarily the formation of C-S-H in hollow-shell separations outside larger alite particles and CH in smaller completely hollow shells, is seen to a much reduced extent when the systems contain csf. This is an important reason for high hollow-shell porosities at later ages in systems with csf.

3.2. Presence of hollow-shell pores, implications for the capillary pore structure, and MIP results

When reaction products do not form within the original cement grain boundaries (i.e., formation of hollow shells), they will form outside, in the capillary pore space. Thus, the formation and preservation of hollow-shell pores imply that the capillary porosity and the sizes of the capillary pores are reduced. A densification of the capillary pore space of the systems with csf is also indicated from Figs. 1–8, most conveniently from the high-magnification images. BSE images of flat specimens reflect the backscattering coefficient of scattered regions. The backscattering coefficient is basically dependent on the atomic number of the elements present and their mass concentration. The higher the atomic number of the elements present in a phase and/or the higher their concentration, the brighter the phase appears in the image. The average atomic number of the elements of the C-S-H outer product phase is lower in the systems with silica fume due to their lower Ca/Si ratio. Despite this, the “outer” C-S-H product phase appears equally or more bright, relative to, for example, the anhydrous phases, thus indicating a higher mass concentration or, in other words, a reduced fine porosity. That the backscattering coefficient is influenced by the fine porosity has been reported by Scrivener [25]. In all these relatively dense specimens with capillary pores too small to be resolved in BSE images, a reduced fine porosity of the “outer” C-S-H phase in the systems with silica fume may very well be due to a reduced capillary porosity. As the degree of hydration is not increased when the systems contain csf [17], a reduced capillary porosity can be understood in terms of a hollow-shell hydration mechanism as discussed, but hardly in terms of a pozzolanic reaction. An increase in the volume of solids providing reduced capillary porosity is not to be expected from the pozzolanic reaction. On the contrary, a certain decrease in volume of the solids would be expected as bound water is apparently released [17,26] and a certain chemical shrinkage will occur when CH and csf combine to C-S-H [11].

As discussed in the Introductory, a number of MIP studies have provided results indicating that csf provides a refinement of the pore structure. To demonstrate that the results obtained previously by MIP are not necessarily in conflict with our results showing the presence of a very significant amount of large hollow-shell pores in systems with csf, we will discuss one of the problems inherent with applying MIP to cement-based materials. MIP relates applied mercury pressure to pore diameter; as the pressure increases smaller pores will be intruded. The amount of mercury intruded at a certain applied pressure is taken as the pore volume of pores with a diameter corresponding to the applied pressure. The theory has been briefly described [10,27]. A serious problem arises if a large pore within a specimen is connected to the surface of the specimen via smaller pores, say a hollow-shell pore connected to the surface of the specimen by smaller gel and capillary pores. The large pore will not be intruded at the pressure corresponding to its own size, but at the higher pressure corresponding to the size of the connecting pores. Thus, the pore volume of the large enclosed pore will be recorded at the pore diameter of the small connecting pores [27]. This gives too high a weight to the smaller pores, whereas the size of the large isolated pore will not be recorded. This phenomenon is often termed the “ink-bottle” effect and may obviously restrict the correctness of pore size distributions obtained by MIP, as noted by Auskern and Horn [27] and Diamond and Leeman [28]. The experiment of Diamond and Leeman may demonstrate this phenomenon. They mercury intruded pastes, with and without entrained air voids, of otherwise identical formulations. The pore size distributions revealed that the air voids were detected by the incremental pore volume recorded by MIP.

However, nearly all of the incremental volume was recorded not in the range of the actual sizes of the air voids, but rather in sizes below the threshold diameter. The air voids were tallied by MIP at diameters approximately three orders of magnitude smaller than their real diameters.

Due to the "ink-bottle" effect, the actual sizes of hollow-shell pores, as with "enclosed" capillary pores and air voids, cannot be recorded from the intrusion of mercury. By also recording the mercury retained under depressuration, it is possible to obtain measures of "ink-bottle" porosities [27]. However, as far as the present authors are aware of, this has not been reported for systems containing csf. Although previously obtained MIP pore size distributions do not reveal large "hollow shells," which would not have been expected as discussed, they generally reveal reduced threshold pore diameters and reduced mercury intrusion when csf replaced parts of the cement [11–15]. They also generally show that, at a range of pressures just above the pressure corresponding to the threshold diameter, the volume of mercury intruded is substantially lower in the mixes with csf, whereas at very high pressures more mercury is intruded into the systems with csf. The reduced threshold pore diameter and the reduced intrusion of mercury at pressures just above the pressure corresponding to the threshold pore diameter indicate a lower capillary porosity and thus a refined capillary pore structure. This is consistent with a greater hollow-shell porosity as discussed. The hollow-shell pores themselves are consistent with the increased intrusion of mercury at the highest pressures. Gel pores and hollow-shell pores, the last which probably are connected to the surface of the specimen via "coarse" gel pores, would not be expected to be intruded until very high pressures are attained. Although MIP results are consistent with the presence of hollow shells, reservations should be made for the possibility that mercury "breaks" its way through dense microstructures and for the influence of specimen preparation (i.e., drying) on the fine pore structure.

4. Conclusions

The microstructure and pore structure of mature cementitious systems, with and without silica fume, have been studied by electron microscopy and desorption isotherms. The results indicate a reduced capillary porosity and the presence of many more hollow-shell pores (i.e., Hadley grains) when silica fume replaces parts of the cement. Hollow-shell pores are in the size range of about 1 to 15 μm and are embedded in cement gel. They appear to be connected to the "continuous" capillary pore system by much smaller gel pores. Re-evaluation of previous MIP results actually supports the observation of greater hollow-shell porosities in systems with silica fume.

Hollow shells are formed primarily at early ages, due to the dissolution of cement grains, and they may remain at later ages. In systems without silica fume, most hollow shells become filled with fresh hydrates at somewhat later ages. However, in systems with silica fume, many hollow shells may persist also at later ages. The formation and preservation of hollow shells implies reduced capillary porosities, as reaction products are deposited in the capillary pore space rather than inside the original cement grain boundaries. The reduction of capillary porosity, to a large extent brought about by the formation and preservation of hollow shells, is hypothesized to be an important reason why silica fume is so efficient in reducing permeability. The large but "enclosed" hollow shells will presumably not contribute much to the transport of matter itself.

Hollow-shell pores seem to largely remain saturated with pore fluid despite self-desiccation effects. The smaller capillary pores desiccate before the larger hollow-shell pores, apparently because the hollow-shell pores are not drained until their small entryway pores (gel pores) are drained.

Acknowledgments

We acknowledge the financial support provided by the Foundation for Swedish Concrete Research and the Swedish research consortium for high-performance concrete. The latter group consists of Cementa, Elkem Materials, Euroc Beton, NCC, Skanska, Strängbetong, and the government authorities BFR and Nutek.

References

[1] K.O. Kjellsen, H.M. Jennings, B. Lagerblad, J Mater Sci 32 (1997) 2921.
[2] G. Verbeck, Bulletin 197, PCA Research and Development Laboratories, Portland Cement Association, Skokie, 1966.
[3] J.H. Taplin, Austr J Appl Sci 10 (1959) 329.
[4] H.M. Jennings, B.J. Dalgleish, P.L. Pratt, J Am Ceram Soc 64 (10) (1981) 567.
[5] H.F.W. Taylor, Adv Cem Based Mater 1 (1993) 38.
[6] S. Diamond, D. Bonen, J Am Ceram Soc 76 (12) (1993) 2993.
[7] D.W. Hadley, The Nature of the Paste-Aggregate Interface, Thesis, Purdue University, West Lafayette, 1972.
[8] K.O. Kjellsen, H.M. Jennings, B. Lagerblad, Cem Concr Res 26 (4) (1996) 593.
[9] K.O. Kjellsen, A. Monsøy, Preparation of flat-polished specimens of high-performance concrete for SEM-backscattered electron imaging and microanalysis, in: L. Jany, A. Nisperos, J. Bayles (Eds.), Proceedings of the 18th International Conference of Cement Microscopy, International Cement Microscopy Association, Duncanville, 1996, pp. 356–364.
[10] D.N. Winslow, S. Diamond, J Mater 5 (3) (1970) 564.
[11] E.J. Sellevold, D.H. Bager, E.K. Jensen, T. Knudsen, Silica fume-cement pastes: Hydration and pore structures, in: O.E. Gjørv, K.E. Løland (Eds.), Proceedings of a Nordic Research Seminar on Condensed Silica Fume in Concrete, Report 82.610, Division of Building Materials, Norwegian Institute of Technology, Trondheim, 1982, pp. 19–50.
[12] R.F. Feldman, H. Cheng-yi, Cem Concr Res 15 (5) (1985) 765.
[13] R.L. Day, B.K. Marsh, Cem Concr Res 18 (1) (1988) 63.
[14] M.H. Zhang, O.E. Gjørv, Cem Concr Res 21 (6) (1991) 1006.
[15] E.J. Sellevold, H. Justnes, High-strength concrete binders, Part B: Nonevaporable water, self-desiccation and porosity of cement pastes with and without condensed silica fume, in: V.M. Malhotra (Ed.), Proceedings of the 4th International Conference on Fly Ash, Silica Fume,

Slag and Natural Pozzolans in Concrete, American Concrete Institute, Detroit, 1992, pp. 891–902.
[16] E. Helsing Atlassi, Influence of silica fume on the pore structure of mortar when measured by water vapour sorption isotherms, in: H.M. Jennings, J. Kropp, K. Scrivener (Eds.), Proceedings of the NATO/RILEM Workshop on the Modeling of Microstructure and Its Potential for Studying Transport Properties and Durability, Kluwer Academic Publishers, Dordrecht, 1994, pp. 257–270.
[17] K.O. Kjellsen, L. Fjällberg, T. Skjetne, Report No. 2:97, Swedish Cement and Concrete Research Institute, Stockholm, 1997.
[18] K.L. Scrivener, The microstructure of concrete, in: J. Skalny (Ed.), Materials Science of Concrete I, American Ceramic Society, Westerville, 1991, pp. 127–161.
[19] E.J. Sellevold, Report No. STF70A92050, SINTEF Civil and Environmental Engineering, Trondheim, 1992 (in Norwegian).
[20] E. Helsing Atlassi, A quantitative thermogravimetric study on the nonevaporable water in mature silica fume concrete, Thesis, Department of Building Materials, Chalmers University of Technology, Gothenburg, 1993.
[21] E. Helsing Atlassi, Nonevaporable water and degree of cement hydration in silica fume-cement systems, in: V.M. Malhotra (Ed.), Proceedings of the 5th International Conference on Fly Ash, Silica Fume, Slag and Natural Pozzolans in Concrete, American Concrete Institute, Detroit, 1995, pp. 703–717.
[22] T.C. Powers, T.L. Brownyard, Bulletin 22, Research Laboratories of the Portland Cement Association, Skokie, 1948.
[23] H.F.W. Taylor, D.E. Newbury, Cem Concr Res 14 (4) (1984) 565.
[24] V. Johansen, N. Thaulow, J. Skalny, Betonw Fertigt Techn 11(62) (1995) 56–68.
[25] K.L. Scrivener, Cem Concr Res 22 (6) (1992) 1224.
[26] M.H. Zhang, O.E. Gjørv, Cem Concr Res 21 (12) (1991) 800.
[27] A. Auskern, W. Horn, J Test Eval 1 (1) (1973) 74.
[28] S. Diamond, M.E. Leeman, Pore size distributions in hardened cement paste by SEM image analysis, in: S. Diamond, S. Mindess, F.P. Glasser, L.W. Roberts, J.P. Skalny, L.D. Wakeley (Eds.), Proceedings of the MRS Symposium Microstructure of Cement-Based Systems/Bonding and Interfaces in Cementitious Materials, Vol. 370, Materials Research Society, Pittsburgh, 1994, pp. 217–226.